Jagannath University Journal of Science
Volume 08, Number II, June 2022, pp. 67–74
https://jnu.ac.bd/journal/portal/archives/science.jsp
ISSN 2224-1698

JnUJSci

Effects of Heat Generation and Absorption in Three-dimensional Unsteady Magnetohydrodynamic Nanofluid Flow on a Porous Rotating Disk

Research Article

Mst. Asiya Khatun

Department of Mathematics, Jagannath University, Dhaka-1100, Bangladesh

Received: 06 March 2022
Accepted: 01 May 2022

Abstract: In this study, we investigate three-dimensional unsteady magnetohydrodynamic nanofluid flow with heat generation and absorption on a porus rotating disk with slip effects. We also observe the effects of the thermophoresis and Brownian motion on this flow. Similarity transformations lead to a system of nonlinear ordinary differential equations. We solved the nonlinear system of equations numerically by incorporating the software MATLAB. To observe the behavior of different fields, for instance, concerning velocity, temperature, and concentration distribution graphically, their graphs are portrayed for different values of different parameters. Furthermore, the computational values for appropriate parameters have been calculated and presented here.

Keywords: *Nanofluids • MHD • Brownian motion • Rotating Disk • Heat Generation/Absorption*

1. Introduction

In the last few decades, the thriving prospects of nanotechnology have captured much attention from scientists, researchers, and engineers to explore different types of fields. Nanofluid is one of the important terms of such development. Nanofluids consist of nanoparticles suspended in water, oil, ethylene glycol, etc. with average sizes below 100 nm. Nanofluids offer important advantages over conventional heat transfer fluids. Nanoparticles used in nanofluids include various materials, such as oxide ceramics (Al_2O_3, CuO), carbide ceramics (SiC, TiC), metals (Cu, Ag, Au, Fe), nitride ceramic (AlN, SiN), semiconductors, etc. A small amount of uniformly radiated and stably suspended guest nanoparticles in the base fluid can make dramatic changes in the thermal properties of the host fluid. Stable and highly conductive nanofluids are usually produced by One-step and two-step methods. Karman (1921) firstly explored the three-dimensional viscous flow occupied by the effects of the uniformly rotating disk having fixed angular velocity. Such kind of flow problem has an important effect in enormous applications like power generators, the dynamics of hurricanes and tornadoes, food processing, geothermal extraction, designing of nuclear reactors, rotor-stator systems in turbines, chemical mixing chambers, the oil recovery process, computer storage devices, and many others. The heat transfer properties for laminar flow due to rotating disk were studied by Millsaps and Pohlhausen (1952). Ackroyd (1978) considered the effect of suction/injection in the Von Karman problem. Attia (1998) discussed the unsteady revolving flow near a permeable surface by using the finite difference approach. He examined heat transfer characteristics prompted by permeable heated disks on steady circulating flow. Hatami et al. (2014)

*Corresponding author: Mst. Asiya Khatun
Email: khasiya06@gmail.com

discuss laminar flow of nanofluid occupied by rotating shrinking disk.

Alam et al. (2015) studied transient thermophoretic particle deposition regarding forced convective heat and mass transfer flow induced by rotating disk. Alam et al. (2016) discussed the numerical study of thermophoresis of transient hydromagnetically forced convective slip flow on a porous rotating disk with. Rahman, and Postelnicu (2010) investigated the effect of thermophoresis on the flow of viscous incompressible fluids in forced convective laminar flow on a rotating disk. Chamkha et al. (2012) discussed the effect of radiation on mixed convection on wedges embedded in nanofluid-filled porous media. Rahman and Eltayeb (2013) discussed radiative heat transfer past a non-linear stretching surface with convective boundary condition in a hydromagnetic nanofluid. Uddin et al. (2016) discussed the broad fundamental evolution of nanofluids, which has been thoroughly discussed by sketching out a gigantic description of the small biosphere of nanofluids. A model was revised by Khan et al. (2017) to study the heat transfer and MHD nanofluid flow due to rotating disks. Hayat et al. (2017) discussed magnetohydrodynamic flow with slip effects of nanofluid concerning a rotating disk. Hayat et al. (2017) studied the best study of the three-dimensional flow of Maxwell nanofluids in a rotating frame. Muhammad et al. (2017) studied a modified model of Darcy-Forchheimer flow for Maxwell nanofluids under convective boundary conditions. Aziz et al. (2018) studied stable 3D MHD viscous nanofluid flow without porous media.

The principal motive of this study is to explain the unsteady magnetohydrodynamic nanofluid flow concerning porous rotating disk with heat generation and absorption. The thermophoretic and Brownian motion effects are also discussed under the consideration of nanoparticles. We also studied the velocity slip, thermal slip, and concentration slip effects. The appropriate boundary condition is developed with the Navier-Stokes equation for slip effects and this condition is also known as slip condition. Along with this boundary condition, we took the governing mathematical problem and solve this problem numerically by using the MATLAB-bvp4c technique. The acquired numerical solutions are plotted and interpreted for different parameters. Finally, the local Nusselt number is a function of heat transfer rate is computed for some parameters of different values and presented below.

Nomenclature:

B_0	Magnetic field	T_∞	Temperature of the ambient fluid
c_p	Specific heat at constant pressure	x, y, z	Dimensional coordinate
C	Volume fraction of Nanoparticle	U_T	Target velocity
C_w	Volume fraction of Nanoparticle at surface disk	B	Heat generation/absorption parameter
C_∞	Ambient volume fraction of nanoparticle	α_m	Thermal diffusivity
D_B	Coefficient of Brownian diffusion	w_w	Suction and Injection velocity
D_T	Thermophoretic diffusion coefficient	ρ	Density
F	Dimensionless form of radial velocity	σ	Electric conductivity
G	Dimensionless form of tangential velocity	θ	Dimensionless temperature
H	Dimensionless form of axial velocity	$(\rho c_p)_p$	Effective heat capacity of nanofluid
M	Magnetic field	μ	Dynamic viscosity
κ	Thermal conductivity	Nu	Nusselt number
r	Cylindrical radial coordinate	α	Velocity slip parameter
Le	Lewis number	β	Thermal slip parameter
Nb	Brownian motion parameter	λ	Unsteadiness parameter
R	Rotational parameter	η	Similarity Variable
Nt	Thermophoresis parameter	φ	Cylindrical tangential coordinate
Nu	Nusselt Number	ϕ	Dimensionless concentration
p	Dimensional pressure	Ω	Angular velocity
P	Dimensionless pressure	γ	Concentration slip parameter
p_∞	Pressure of ambient fluid	Ec	Eckert number
Pr	Prandtl number	υ	Kinematic viscosity
Re	Reynolds number	δ	Time dependent length scale
T	Temperature	λ^*	Mean free path
T_w	Temperature at the surface of the disk	$(\rho c_p)_f$	Heat capacity of fluid

2. Mathematical Modeling

The components of the flow velocity u,v,w are in the direction of (r,φ,z) respectively are shown in fig. 1. The surface magnetic field B_0 is applied perpendicular to the surface in the fluid.The surface temperature of the rotating disk is uniform and the free flow temperatures are T_w and T_∞ ($T_w > T_\infty$) respectively. The fluid is at rest when, as a result, the disk does not rotate, and the fluid has a constant temperature and concentration. When t = 0 and in the case of constant angular velocity, the disk is in motion. For a very short time interval, the flow is also transient before having steady state position. To understand the variation of mass deposition on the surface, Brownian motion and thermophoresis effects are being considered. In this study, we take the nanofluid as a mixture of two components such as base fluid and nanoparticle. For this study, we also assume other conditions such as (i) incompressibility, (ii) no chemical reaction, (iii) dilute mixture, (iv) viscous dissipation, (v) nanoparticles, and the base fluid locally in thermal equilibrium. By using the mentioned hypothesis, the governing equation for the present investigation is coupled by the partial differential equation (see also Buongiorno (2006) and Hayat et al. (2017)

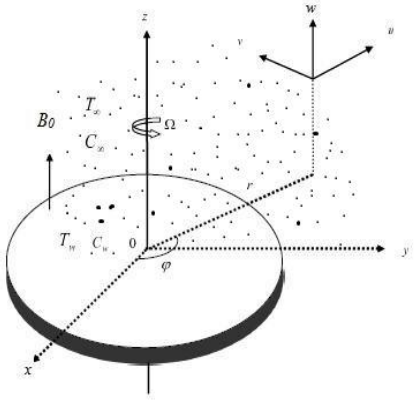

Figure 1: Physical model of the flow.

$$\frac{\partial u}{\partial \mathrm{r}} + \frac{u}{r} + \frac{\partial w}{\partial z} = 0 \tag{1}$$

$$\frac{\partial u}{\partial \mathrm{t}} + u\frac{\partial u}{\partial r} - \frac{v^2}{r} + w\frac{\partial u}{\partial z} = -\frac{1}{\rho}\frac{\partial \rho}{\partial r} + \upsilon\left(\frac{\partial^2 u}{\partial r^2} + \frac{1}{r}\frac{\partial u}{\partial r} - \frac{u}{r^2} + \frac{\partial^2 u}{\partial z^2}\right) - \frac{\sigma B_0^2 u}{\rho} \tag{2}$$

$$\frac{\partial v}{\partial \mathrm{t}} + u\frac{\partial v}{\partial r} + \frac{uv}{r} + w\frac{\partial v}{\partial z} = \upsilon\left(\frac{\partial^2 v}{\partial r^2} + \frac{1}{r}\frac{\partial v}{\partial r} - \frac{v}{r^2} + \frac{\partial^2 v}{\partial z^2}\right) - \frac{\sigma B_0^2 v}{\rho} \tag{3}$$

$$\frac{\partial w}{\partial \mathrm{t}} + u\frac{\partial w}{\partial r} + \frac{uv}{r} + w\frac{\partial u}{\partial z} = -\frac{1}{\rho}\frac{\partial \rho}{\partial z}\upsilon\left(\frac{\partial^2 w}{\partial r^2} + \frac{1}{r}\frac{\partial w}{\partial r} + \frac{\partial^2 w}{\partial z^2}\right) \tag{4}$$

$$\frac{\partial T}{\partial \mathrm{t}} + u\frac{\partial T}{\partial r} - \frac{v^2}{r} + w\frac{\partial T}{\partial z} = \alpha_m\left(\frac{\partial^2 T}{\partial r^2} + \frac{1}{r}\frac{\partial T}{\partial r} + \frac{\partial^2 T}{\partial z^2}\right) + \frac{(\rho c_p)_p}{(\rho c_p)_f}\left[D_B\left(\frac{\partial C}{\partial z}\frac{\partial T}{\partial z} + \frac{\partial C}{\partial r}\frac{\partial T}{\partial r}\right) + \frac{D_T}{T_\infty}\left(\left(\frac{\partial T}{\partial r}\right)^2 + \left(\frac{\partial T}{\partial z}\right)^2\right)\right] + \frac{Q}{(\rho c_p)_f}(T - T_\infty) + \frac{\mu}{(\rho c_p)_f}[2\left\{\left(\frac{\partial u}{\partial r}\right)^2 + \left(\frac{u}{r}\right)^2 + \left(\frac{\partial w}{\partial z}\right)^2\right\} + \left(r\frac{\partial}{\partial r}\left(\frac{v}{r}\right)\right)^2 + \left(\frac{\partial v}{\partial z}\right)^2 + \left(\frac{\partial u}{\partial z} + \frac{\partial w}{\partial r}\right)^2] \tag{5}$$

$$\frac{\partial C}{\partial \mathrm{t}} + u\frac{\partial C}{\partial r} + w\frac{\partial C}{\partial z} = D_B\left(\frac{\partial^2 C}{\partial r^2} + \frac{1}{r}\frac{\partial C}{\partial r} + \frac{\partial^2 C}{\partial z^2}\right) + \frac{D_T}{T_\infty}\left(\frac{\partial^2 T}{\partial r^2} + \frac{1}{r}\frac{\partial T}{\partial r} + \frac{\partial^2 T}{\partial z^2}\right) \tag{6}$$

Where μ is the dynamic viscosity, ρ is the density of base fluid, kinematic viscosity = $\frac{\mu}{\rho}$, σ is the electrical conductivity, thermal diffusivity $\alpha_m = \frac{\kappa}{(\rho c_p)_f}$, thermal conductivity κ, heat capacity is presented by $(\rho c_p)_f$ of fluid, effective heat capacity $(\rho c_p)_p$ of nanoparticles, D_B is the coefficient of Brownian diffusion and D_T presents the thermophoretic diffusion coefficient.

2.1. Conditions at the Boundary

(i) At $z = 0$ on disk's surface

$$\left.\begin{aligned} \mathrm{u} = \mathrm{L}_1\frac{\partial \mathrm{u}}{\partial \mathrm{z}}, \mathrm{v} = \Omega \mathrm{r} + \mathrm{L}_1\frac{\partial \mathrm{v}}{\partial \mathrm{z}}, \mathrm{w} = \mathrm{w_s} \\ \mathrm{p} = 0, \mathrm{T} = \mathrm{T_w} + \mathrm{L}_2\frac{\partial \mathrm{T}}{\partial \mathrm{z}} \\ \mathrm{C} = \mathrm{C_w} + \mathrm{L}_3\frac{\partial \mathrm{C}}{\partial \mathrm{Z}} \text{ at } \mathrm{z} \to 0 \end{aligned}\right\} \tag{7}$$

(ii) For free stream $z \to \infty$

$$\left.\begin{aligned} u = 0, v = 0, p \to p_\infty \\ T \to T_\infty, C \to C_\infty \; as \; z \to \infty \end{aligned}\right\} \tag{8}$$

3. Dimensionless Governing Equations

From governing equations (1)–(6) and the boundary conditions (7)–(8) for obtaining the similarity transformations we define the following appropriate similarity transformations:

$$\left.\begin{aligned} \eta = \frac{z}{\delta}, u = \Omega r F(\eta), v = \Omega r G(\eta) \\ w = \frac{\vartheta}{\delta}H(\eta), P = -\rho\vartheta\Omega P(\eta) \\ \theta(\eta) = \frac{T - T_\infty}{T_w - T_\infty}, \phi(\eta) = \frac{C - C_\infty}{C_w - C_\infty} \end{aligned}\right\} \tag{9}$$

where scale factor $\delta = \delta(t)$ is the function of the time.

Substituting (9) into equations (1)–(6) leads to the following coupled differential equations:

$$H' + 2RF = 0 \tag{10}$$

$$F'' - HF' - R(F^2 - G^2) + \lambda\eta F' - MF = 0 \tag{11}$$

$$G'' - HG' - 2RFG + \lambda\eta G' - MG = 0 \tag{12}$$

$$H'' - HH' + RP' + \lambda\eta H' = 0 \quad (13)$$

$$\theta'' - PrH\theta' + Pr\lambda\eta\theta' + Nb\theta'\phi' Pr + Nt\theta'^2 Pr + Pr\theta B + PrEc(F'^2 + G^2) + \left(\frac{1}{Re}\right)^2 (2H'^2 + 4R^2F^2) = 0 \quad (14)$$

$$\phi'' + Le\lambda\eta\theta' - LeH\phi' + \frac{Nt}{Nb}\theta'' = 0 \quad (15)$$

Transformed boundary conditions for the present problem are considered as follows

$$\left.\begin{array}{c} F = \alpha F', G = \alpha G' \\ H = w_w, P = 0, \theta = 1 + \beta\theta' \\ \phi = 1 + \gamma\phi' \text{at } \eta = 0 \end{array}\right\} \quad (16)$$

$$F = 0, G = 0, \theta = 0, \phi = 0 \text{ as } \eta \longrightarrow \infty \quad (17)$$

where $W_w = \frac{w_s\delta}{\nu}$ is the suction ($w_w < 0$) or injection ($w_s > 0$) at the surface, rotational parameter $R = \frac{\Omega\delta^2}{\nu}$, unsteadiness parameter $\lambda = \frac{\delta}{\nu}\frac{d\delta}{dt}$, $Pr = \frac{\nu}{a_m}$ presents the Prandtl number, $Nt = \frac{\tau D_T \Delta T}{T\infty\nu}$ is the thermophoresis parameter, $Nb = \frac{\tau D_B \Delta C}{\nu}$ represents Brownian diffusion, velocity slip $\alpha = \frac{L_1}{\delta}$, thermal slip $\beta = \frac{L_2}{\delta}$ and concentration slip $\gamma = \frac{L_3}{\delta}$, $B = \frac{Q\delta^2}{\nu(\rho c_p)_f}$ is the heat generation/absorption, $Le = \frac{\nu}{D_B}$ is the Lewis number, $Ec = \frac{\Omega^2 r^2}{cp\Delta T}$ is Eckert Number, $Re = \frac{\delta\Omega r}{\nu}$ is Reynolds number and $M = \frac{\alpha_{mB0}^2\delta^2}{p\nu}$ is the magnetic field parameter.

4. Rate of heat transfer

Here Fourier's law is used to calculate the heat transfer rate from the disk surface to the nanofluid as follows

$$q_w = -\kappa\frac{\partial T}{\partial z_{z=0}} = \kappa\frac{T_\infty - T_w}{\delta}\theta'(0)$$

Here the Nusselt number Nu is obtained in the form of

$$Nu = \frac{\delta q_w}{\kappa(T_\infty - T_w)} = -\theta'(0)$$

5. Validity of code

When λ=0 (i.e.considering the steady-state situation), R=1, M = 0, $W_w = 0$, α = β = γ = 0 ignoring the effect of heat and mass transfer,the current work is in good agreement with White [18].To evaluate the exactness of the current study, we need to calculate the values of F, G and H for some values of with no presence of heat and mass transfer value. We can see the comparison of data of this study and those data obtained by White [18] from Table 1. It is vividly noticed that there are very stunning consistencies exist between the results. This comparison helps us for acquiring confidence in the present numerical approach.

Table 1. Displays numerical values of $F(\eta), G(\eta)$and $-H(\eta)$ without heat and mass transfer and for $\lambda = M = w_w = \alpha = \beta = \gamma = 0$ and R = 1.

η	$F(\eta)$		$G(\eta)$		$-H(\eta)$	
	White (1991)	Present work	White (1991)	Present Work	White (1991)	Present work
0.0	0.0000	0.0000	1.0000	1.0000	0.0000	0.0000
1.0	0.1801	0.1801	0.4766	0.4767	0.2655	0.2656
2.0	0.1188	0.1185	0.2034	0.2036	0.5732	0.5726
3.0	0.0581	0.5656	0.0845	0.0842	0.7452	0.7440
4.0	0.0256	0.0257	0.0349	0.0345	0.8249	0.8237
5.0	0.0108	0.0105	0.0144	0.0135	0.8594	0.8561

6. Approach of Numerical Solutions

The set of equations (10)-(15) cannot be solved analytically because they are highly nonlinear and incorporated. Equation (13) is used for calculating pressure, we can cancel this equation from the system as the pressure H is known from the other equations. By using MATLAB, we can solve the transformed governing equations (10)-(12) and (14)-(15) with boundary conditions (16)-(17) numerically. It is well known that the software is very effective, and it can be applied successfully for solving a wide variety of nonlinear fluid flow problems.

7. Results and Discussion

To discuss the results, the computations are shown graphically for dimensionless velocity, temperature, and concentration as well whereas the tabular form also presents the rates of heat transfer. Due to the lack of experimental datum, the selection of parameters is introduced by previous investigators. In the current investigation, we deemed gaseous nanofluid which

contains (Cu, Al_2O_3, TiO_3, etc. nanoparticles). The value of $\Pr = 5$ is surmised in this investigation.

The velocity distribution for some selected values of the velocity slip parameter is shown in Figure 2. This figure shows that the radial velocity distribution decreases as the value of the velocity slip parameter increases. Therefore, velocity slip results in a deceleration force that reduces the velocity boundary layer.

Figure 3 displays the manner of tangential velocity. As seen in Figure 2, for the large values of velocity slip parameter, the velocity boundary layer is also inhibited by a retardation force. This is because the velocity slip parameter mainly slows the fluid motion, which effectively confirms the reduction in the net motion of fluid particles. Therefore, less particle motion results in a reduction in the velocity field.

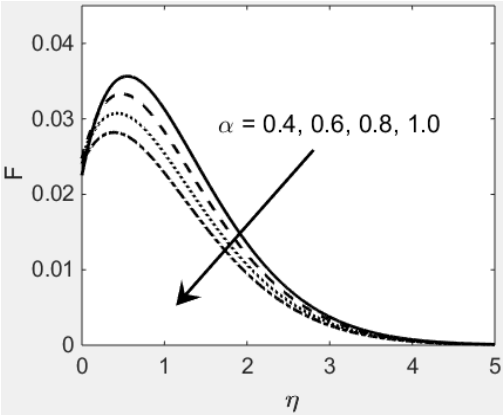

Figure 2. Radial velocity profile for α.

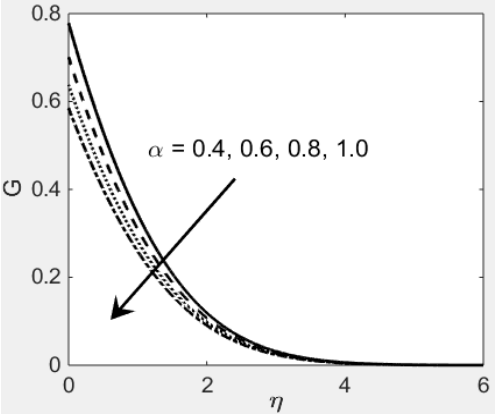

Figure 3. Tangential velocity profile for α.

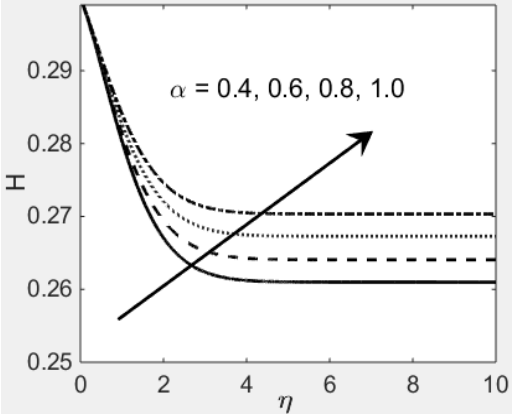

Figure 4. Axial velocity profile for α.

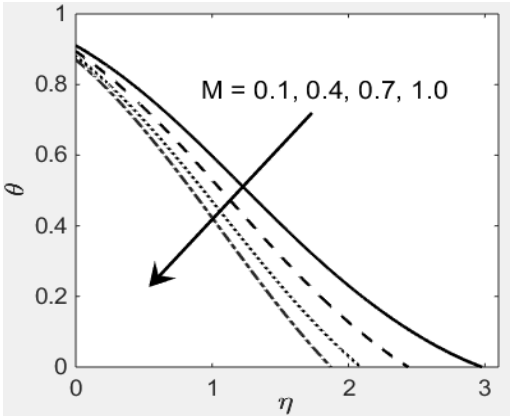

Figure 5. Temperature profile for M.

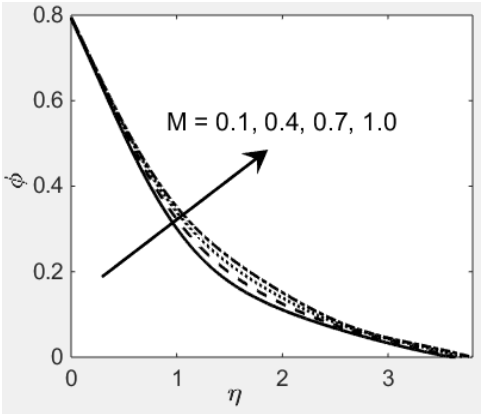

Figure 6. Concentration profile for M.

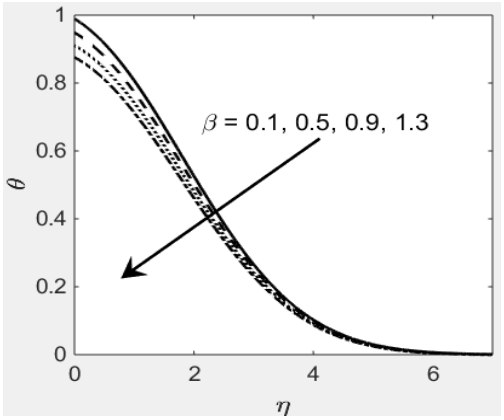

Figure 7. Temperature profile for β.

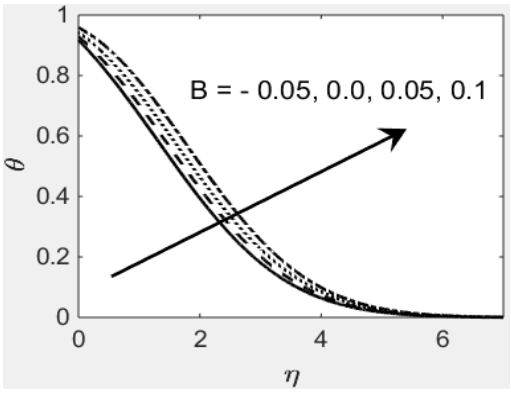

Figure 8. Temperature profile for B.

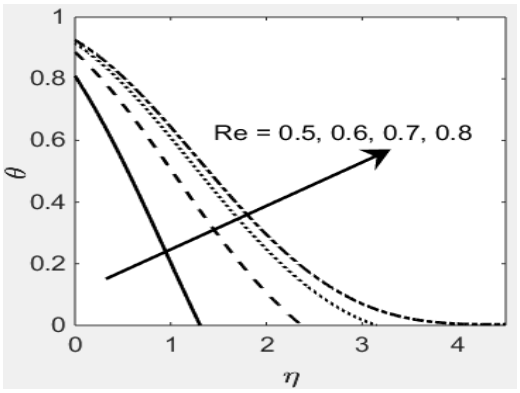

Figure 9. Temperature profile for Re.

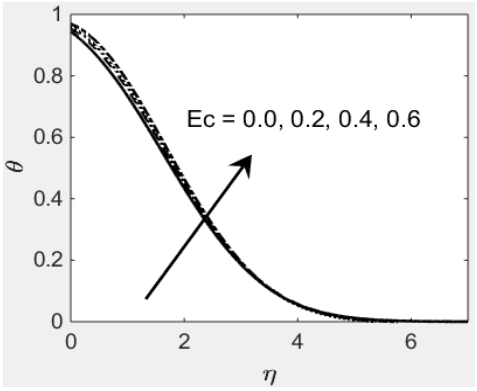

Figure 10. Temperature profile for Ec.

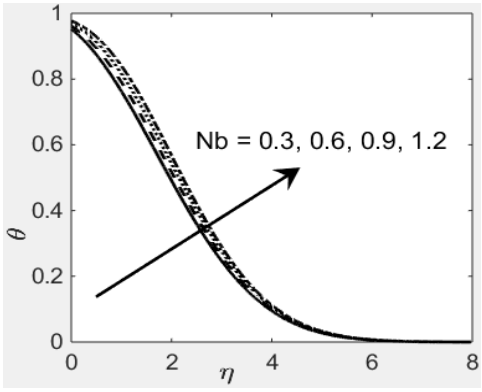

Figure 11. Temperature profile for Nb.

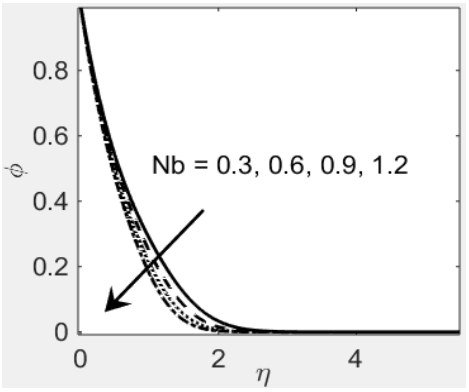

Figure 12. Concentration profile for Nb.

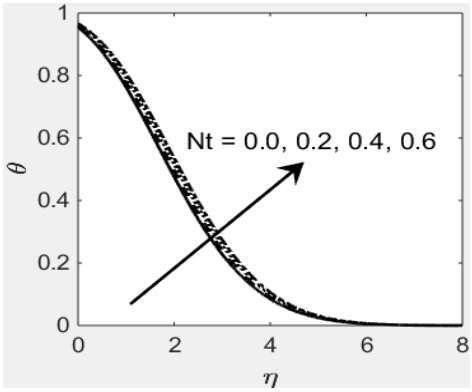

Figure 13. Temperature profile for Nt.

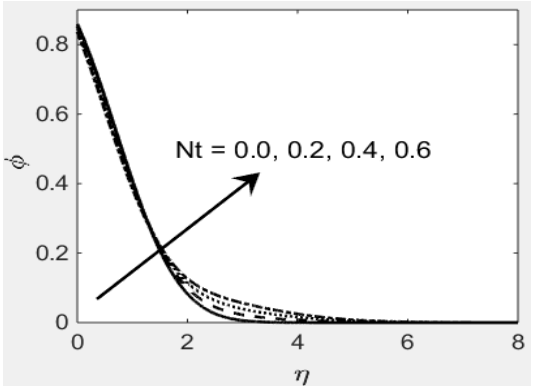

Figure 14. Concentration profile for Nt.

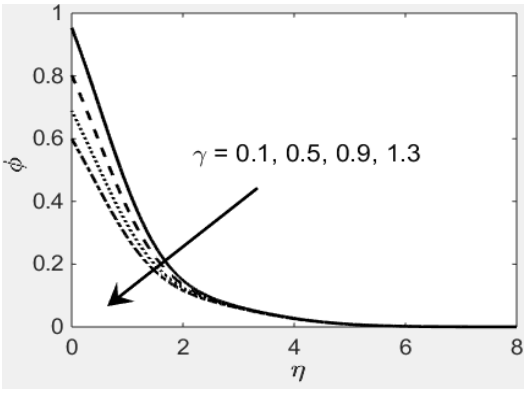

Figure 15. Concentration profile for γ.

Figure 4 depicts the behaviors of axial velocity. The negative values of H are denoting downward fluidic flow in the direction of vertically. So, the incremented of M shows a decreasing trend. It implies that the flow intensity is decreased vertically for the presence of magnetic force.

It can be said from Figure 5 that the temperature of the fluidic flow inside the boundary layer is intensified with the increment of the magnetic field M. The magnetic parameter is the ratio of electromagnetic force to the viscous force and is used to evaluate the strength of the magnetic force exerted in the medium. The rise of the magnetic force together with the slip effects, acts as a retarding force as a result, It decreases the temperature profile as the value of the magnetic field M increases. It can be predicted from Figure 6 because the magnetic field M widens the concentration distribution. The value of the magnetic field M is proportional are to the concentration distribution. There fore a higher value of the magnetic field M means an increase in concentration.

The temperature field effect of thermal slip parameters is sketched in Figure 7. This Figure delineates that with the increment of the values of thermal slip emerges a force that causes the temperature field to be reduced. Figure 8 portrays how the temperature profile is affected by heat generation and absorption parameters. Here the heat generation happens for the values of $B > 0$, and the heat absorption occurs when $B < 0$. The thermal layer thickness and temperature are augmented for the enlarged values of B.

The temperature profiles are pictured in Figure 9 for some chosen values of Reynolds number Re. We know that the Reynolds number presents the ratio of inertial forces to viscous forces. Increasing values of Reynolds number leads to the intensified thermal boundary layer. Figure 10 portrays how the temperature field is affected by the changes in the Eckert number Ec. It is noted that the Eckert number is used to compute how intense the effect of viscous dissipation. An increment of the temperature distribution profile is noticed when the Eckert number is increased. We can see that from the figure, the reverse heat flow near the horizontal portion of the disk when the Eckert number is relatively large.

It is depicted in Figure 11 how the Brownian motion parameter make an effect on the temperature profile distribution. From the physics of Brownian motion, it causes random motion of nanoparticles. The more values of Brownian motion lead the more random motion. Consequently, more heat energy emerges from more kinetic energy that causes temperature profile and thermal layer thickness to be augmented

From Figure 12, it appears that the concentration layers are squeezed with the augmented values of the Brownian motion. The Brownian motion emerges as a force to circulate the nanoparticles in the countermand direction of the rate of changes of concentration and consequently, nanofluid becomes a homogenous type. Therefore, the larger Brownian motion forces imply a lower rate of changes of concentration inside the boundary layer. Figure 13 portraits the growing values of the thermophoresis parameter leading to the temperature distribution profile to be experienced an upward trend. For greater values of this parameter provides a more intense force (thermophoretic) that helps to move the nanoparticles from the hooter region to the cooler region. This movement results in an increase to the thickness of the thermal boundary layer and temperature distribution.

From Figure 14, the effect of the thermophoresis parameter is observed on the concentration profile. With the increasing value of this parameter, concentration distribution is increased. Physically, the thermophoretic force causes the shifting of nanoparticles in the reverse direction of the rate of change of temperature, causing a concentration distribution (non-uniform). It is inferred that the more thermophoretic force leads the more rate of changes of concentration indicating more concentration profiles (non-uniform).

Table 2. Variations of local Nusselt Number for some selected values of Nt, Nb and M.

Nt	Nb	M	$-\theta'(0)$
0.1			0.1930
0.3	0.5	0.5	0.1554
0.5			0.1348
0.7			0.1246
	0.1		0.3843
	0.3		0.2897
0.5	0.5	0.5	0.1348
	0.7		0.1175
		0.1	0.31471
0.5	0.5	0.4	0.31929
		0.7	0.35549
		1.0	0.41299

From Figure 15, it is perceived the concentration slip parameter influences concentration. The concentration distribution is lower for large concentration slip parameters. Since if the temperature inside the flow can be controlled by the thermal slip parameter, then it is quite possible that the concentration slip parameter can control the mass transport phenomenon.

Table 2 presents the heat transfers rate for varying values of thermophoresis, Brownian diffusion, and magnetic field parameter. From this table, we can see the heat transfer rate is lower as long as the larger values of the thermophoresis parameter prevail. The rates of heat transfer are also lowered according to the stronger Brownian motion parameter. The inverse demand trend is shown in the heat transfer rate for some selected increasing values of M.

Conclusion

The effects of the unsteady nano-magnetohydrodynamic nanofluid flow on a rotating disk due to slip condition and the effects of heat generation/absorption are taken into consideration in this present work. The main inspections are indicated as follows:

- An increase in the value of velocity slip parameter results in a decrease in the value of radial, tangential, and axial velocity distributions.
- For larger magnetic field parameters, the opposite behavior of the temperature and concentration curves is shown.
- An increase in the thermal slip parameter value indicates a lower temperature profile.
- For larger values of heat generation/absorption parameter, the upward trend is observed in the thermal boundary layer.
- A larger Reynolds number causes the enhancement of the temperature profile.
- As the Eckert number increases, so does the temperature distribution and its associated thermal boundary layer thickness.
- For large Brownian motion causes the temperature and concentration profiles to have opposite behaviors.
- Enlarged thermophoresis parameter reveals alike characteristics for both cases of temperature and concentration as well.
- A larger concentration slip parameter depicts the squeezed trend in the concentration profile.

References

Ackroyd JAD, 1978. On the steady flow produced by a rotating disk with either surface suction or injection. *J Eng Math.*12: 207-220.

Alam MS, Chapal Hossain SM, and Rahman MM., (2015). Transient thermophoretic particle deposition on forced convective heat and mass transfer flow due to a rotating disk, *Ain Shams Engineering Journal*, 7: 441-452.

Alam MS, Rahman MM, Rahman MM, Uddin MJ, Vajravelu K., (2016). Numerical study of transient hydromagnetic forced convective slip flow over a porous rotating disk with thermophoresis. *J. Nonl. Evol. Equ. Appl*. 2016(1): 1-23.

Attia HA, (1998). Unsteady MHD flow near a rotating porous disk with uniform suction or injection. *Fluid Dyn Res*, 23:283–290.

Aziz A., Alsaedi A., Muhammad T., Hayat T., (2018). Numerical study for heat generation/absorption in flow of nanofluid by a rotating disk. *Results in Physics.* 8: 785-792,

Buongiorno J., (2006). Convective transport in nanofluids. *ASME J. Heat Trans.* 128:240-250.

Chamka AJ, Abbasbandy S., Rashad AM. (2012). Radiation Effects on Mixed Convection over a Wadge Embedded in a Porous Medium Filled with a Nanofluid. *Transp Porous Med*, 91: 261-279.

Hatami M., Sheikholeslami M., Ganji DD, (2014). Laminar flow and heat transfer of nanofluid between contracting and rotating disks by least square method. *Powder Technol*, 253: 769-779.

Hayat T., Muhammad T., Shehzad SA, Alsaedi A., (2017). On magnetohydrodynamic flow of nanofluid due to a rotating disk with slip effect: *A numerical study, Computer Methods in Applied Mechanics and Engineering*, 315: 467-477.

Hayat T., Muhammad T., Shehzad SA, Alsaedi A., (2017). Three-dimensional rotating flow of Maxwell nanofluid, *Journal of Molecular Liquids*, 229: 495-500.

Khan JA, Mustafa M., Hayat T., Turkyilmazoglu M. and Alsaedi A. (2017). Numerical study of nanofluid flow and heat transfer over a rotating disk using Buongiorno's model. *International Journal of Numerical Methods for Heat & Fluid Flow*, 27: 221-234.

Millsaps K, Pohlhausen K, (1952). Heat transfer by laminar flow from a rotating disk. *J Aeronaut Sci*, 19:120–126.

Muhammad T., Alsaedi A., Hayat T., Shehzad SA, 2017. A revised model for Darcy-Forchheimer three-dimensional flow of nanofluid subject to convective boundary condition, *Results in Physics*. 7: 2791-2797.

Rahman MM, Postelnicu A. (2010). Effects of thermophoresis on the forced convective laminar flow of a viscous incompressible fluid over a rotating disk, *Mechanics Research Communications*, 37:598-603.

Rahman MM, Eltayeb IA, (2013). Radiative heat transfer in a hydromagnetic nanofluid past a non- linear stretching surface surface with convective boundary condition. *Meccanica*,48:601-615

Uddin, MJ, Kalbani KS, Rahman MM, Alam MS, Al-Salti N., & Eltayeb IA, (2016). Fundamentals of nanofluids evolution, applications and new theory, *International Journal of Biomathematics and Systems Biology.*

Von Karrman T. (1921). Uberlaminare und turbulentereibung. *Z Angew Math Mech*, 1:233–252.

White FM, (1991). Viscous fluid flows, McGraw-Hill, Inc., New York.